

COMPLEX SPECTRAL VARIABILITY FROM INTENSIVE MULTIWAVELENGTH MONITORING OF MARKARIAN 421 IN 1998

T. TAKAHASHI,^{1,2} J. KATAOKA,^{1,2} G. MADEJSKI,^{3,4} J. MATTOX,⁵ C. M. URRY,⁶ S. WAGNER,⁷ F. AHARONIAN,⁸ M. CATANESE,⁹
L. CHIAPPETTI,¹⁰ P. COPPI,¹¹ B. DEGRANGE,¹² G. FOSSATI,¹³ H. KUBO,¹⁴ H. KRAWCZYNSKI,⁸ F. MAKINO,¹ H. MARSHALL,¹⁵
L. MARASCHI,¹⁶ F. PIRON,¹² R. REMILLARD,¹⁵ F. TAKAHARA,¹⁷ M. TASHIRO,² H. TERASRANTA,¹⁸ AND T. WEEKES⁹

Received 2000 June 7; accepted 2000 August 17; published 2000 October 4

ABSTRACT

We conducted a multifrequency campaign for the TeV blazar Markarian 421 in 1998 April. The campaign started from a pronounced high-amplitude flare recorded by *BeppoSAX* and Whipple; the *ASCA* observation started 3 days later. In the X-ray data, we detected multiple flares, occurring on timescales of about 1 day. *ASCA* data clearly reveal spectral variability. The comparison of the data from *ASCA*, the *Extreme Ultraviolet Explorer*, and the *Rossi X-Ray Timing Explorer* indicates that the variability amplitudes in the low-energy synchrotron component are larger at higher photon energies. In TeV γ -rays, large intraday variations—which were correlated with the X-ray flux—were observed when results from three Cerenkov telescopes were combined. The rms variability of TeV γ -rays was similar to that observed in hard X-rays, above 10 keV. The X-ray light curve reveals flares that are almost symmetric for most cases, implying that the dominant timescale is the light crossing time through the emitting region. The structure function analysis based on the continuous X-ray light curve of 7 days indicates that the characteristic timescale is ~ 0.5 days. The analysis of *ASCA* light curves in various energy bands appears to show both soft (positive) and hard (negative) lags. These may not be real, as systematic effects could also produce these lags, which are all much smaller than an orbit. If the lags of both signs are real, these imply that the particle acceleration and X-ray cooling timescales are similar.

Subject headings: BL Lacertae objects: general — BL Lacertae objects: individual (Markarian 421) —
X-rays: general

1. INTRODUCTION

According to well-established unified schemes for radio-loud active galactic nuclei (AGNs; Urry & Padovani 1995), blazars are distinguished by the fortuitous alignment of their jets along the line of sight. This greatly enhances the jet radiation, making them ideal sources for understanding jet physics in all radio-loud AGNs. The required high energies of the radiating electrons indicate very efficient particle acceleration in the relativistic jets of these sources (Kubo et al. 1998; Ghisellini et al. 1998).

The BL Lac object Markarian 421 is unique as the first—and so far, the brightest—high-frequency-peaked BL Lac objects

(HBLs) with γ -ray emission extending up to TeV energies, at a level allowing detailed spectral and variability studies in the broadest spectral range. The simple continuum spectra of Mrk 421 from radio to UV and X-ray bands obtained previously imply that the emission in these energy bands is due to charged particles radiating via the synchrotron process (e.g., George, Warwick, & Bromage 1988). The hard X-rays and γ -rays from this object are likely to be produced by inverse Compton scattering of synchrotron photons by the same electrons (e.g., Ulrich, Maraschi, & Urry 1997 and references therein). Judging from the results of previous TeV and multiwavelength monitoring campaigns of Mrk 421, correlations among light curves at different energies (and, in particular, the pronounced spectral evolution during flares seen in X-rays) have provided our best opportunity to understand the high-energy emission from blazar jets (Macomb et al. 1995; Buckley et al. 1996; Takahashi et al. 1996; Takahashi, Madejski, & Kubo 1999; Wagner 1996). Specifically, the previous (1994) campaigns found a soft lag of about 4000 s for soft X-ray (0.5–1.0 keV) photons with respect to the hard X-ray (2–7.5 keV) band, which was interpreted as an effect of radiative cooling (Takahashi et al. 1996). However, the sparse sampling of previous campaigns has prevented us from obtaining definitive conclusions. Uninterrupted monitoring, lasting several times the characteristic timescale, is the only way to investigate quantitatively the extreme physical conditions at the sites of high-energy radiation.

Accordingly, we carried out a 1 week continuous observation with *ASCA*, coordinated with the *Extreme Ultraviolet Explorer* (*EUVE*), the *Rossi X-Ray Timing Explorer* (*RXTE*), and *BeppoSAX*. At the same time, TeV detectors [Cerenkov Array at Themis (CAT), High-Energy Gamma-Ray Astronomy (HEGRA), and Whipple], optical telescopes, radio antennae at 22 and 37 GHz, attempted to monitor the source every night.

¹ Institute of Space and Astronautical Science, 3-1-1 Yoshinodai, Sagamiharashi, Kanagawa 229-8510, Japan.

² Department of Physics, University of Tokyo, Tokyo 113-0033, Japan.

³ NASA Goddard Space Flight Center, Laboratory for High-Energy Astrophysics, Greenbelt, MD 20771.

⁴ Department of Astronomy, University of Maryland, College Park, MD 20742.

⁵ Astronomy Department, Boston University, Boston, MA 02215.

⁶ Space Telescope Science Institute, Baltimore, MD 21218.

⁷ Landessternwarte Heidelberg, Königstuhl, D-69117 Heidelberg, Germany.

⁸ Max-Planck-Institut für Kernphysik, D-69029 Heidelberg, Germany.

⁹ Fred Lawrence Whipple Observatory, Harvard-Smithsonian Center for Astrophysics, Amado, AZ 85645.

¹⁰ Istituto di Fisica Cosmica CNR, Milano, Italy.

¹¹ Department of Astronomy, Yale University, New Haven, CT 06520-8101.

¹² Laboratoire de Physique Nucléaire des Haute Énergies, École Polytechnique Palaiseau, France.

¹³ Center for Astrophysics and Space Sciences, University of California at San Diego, La Jolla, CA 92093-0424.

¹⁴ Department of Physics, Tokyo Institute of Technology, Tokyo, 152-8551, Japan.

¹⁵ Center for Space Research, Cambridge, MA 02139.

¹⁶ Osservatorio Astronomico di Brera, 20121 Milano, Italy.

¹⁷ Department of Earth and Space Science, Osaka University, Osaka, Japan.

¹⁸ Metsähove Radio Observatory, Kylmala, Finland.

In this Letter, we present only the most important result of the multiwavelength campaign.

2. OBSERVATIONS AND RESULTS

2.1. Observations

The essential information on the observations is summarized in Figure 1, which shows the normalized multiwavelength (EUV, X-ray, and TeV) light curves. The logarithmic flux scale allows flares with equal amplitudes to be represented by equal vertical excursions. Complete details about the data analyses will be given in separate wavelength-based papers (Aharonian et al. 1999; Fossati et al. 2000a, 2000b; Kataoka et al. 2000a); here we summarize the key points.

Continuous coverage in X-rays with *ASCA* lasted from 1998 April 23.97 to 30.8 UT, yielding a net exposure of ~ 280 ks. The results presented here are from the Solid-State Imaging Spectrometer (SIS) detectors operated in 1-CCD mode because the count rate of the Gas Imaging Spectrometer detectors exceeded its telemetry limit for 20%–30% of the observation time. The background count rate and its fluctuations are negligible, so we did not perform any background subtraction so as to avoid any artificial effects.

BeppoSAX observations of Mrk 421 preceded the *ASCA* observation by about 3 days (Maraschi et al. 1999). The *RXTE* observed the source primarily only in low-background orbits in order to minimize uncertainties in the background subtraction. *EUVE* observations covered the whole campaign, lasting from April 19.4 to May 1.2. The γ -ray observations at TeV energies were made with the CAT, HEGRA, and Whipple atmospheric Cherenkov telescopes. Optical observations with *BVRI* filters were performed by the WEBT collaboration (J. Mattox et al. 2000, in preparation). Radio observations were done at the Metsähovi Radio Observatory (Teräsanta et al. 1998).

2.2. Multiwavelength Light Curves

The campaign began during a pronounced high-amplitude flare recorded simultaneously by *BeppoSAX* and Whipple (Maraschi et al. 1999), and the high activity of Mrk 421 continued throughout the campaign (Fig. 1). The 2–10 keV flux at the beginning of the *ASCA* observation was 1.2×10^{-10} ergs $\text{cm}^{-2} \text{s}^{-1}$ and increased to 5.0×10^{-10} ergs $\text{cm}^{-2} \text{s}^{-1}$ at the maximum. Thanks to the continuous coverage with *ASCA*, the X-ray variations are fully resolved *with no gaps*. Many “flares” are seen clearly in the *ASCA* data, superposed on a general increasing trend. The *EUVE* light curve also shows a series of flares, less well defined because of lower amplitude and lower signal-to-noise ratio but well correlated in time with the X-ray flares. The optical data for the period April 24–30 indicate an *R*-band flux with a mean value of 12.6 mag and variability of less than 0.1 mag about this mean. The high-frequency radio flux did not change within statistics; the mean fluxes during the Metsähovi observations are 0.5 Jy for 22 GHz (April 20–26) and 0.6 Jy for 37 GHz (April 18–21).

In Mrk 421, the EUV through X-ray emission comprises the high-energy part of the synchrotron component. Comparison of the data from *ASCA*, *EUVE*, and *RXTE* indicates that the variability amplitude in the synchrotron component increases with photon energy. To show this quantitatively, we computed the fractional rms variability including the general, increasing trend. The calculated rms variability during the *ASCA* campaign increases with energy, from 0.158 ± 0.007 in the *EUVE* light

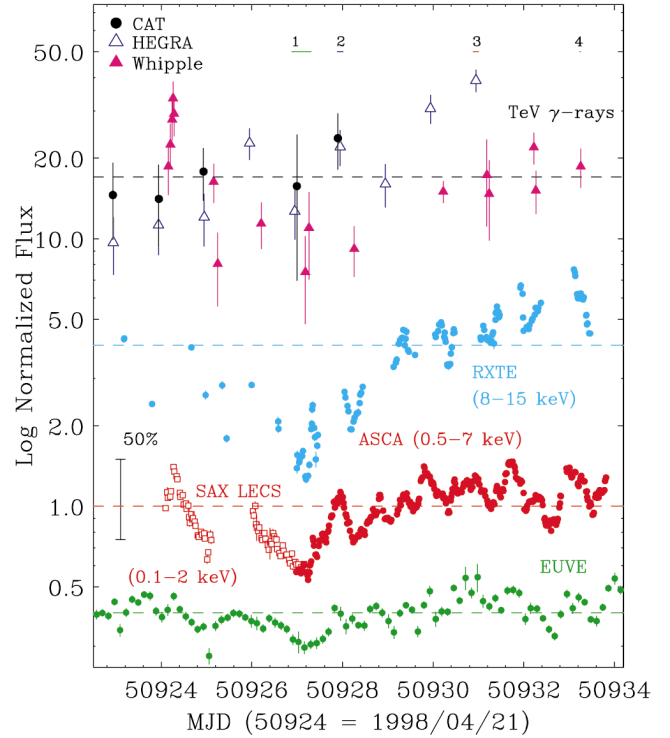


FIG. 1.—Multiwavelength light curve for the 1998 campaign for Mrk 421. The *ASCA* light curve is extracted by integrating photons within 1'0 and 2'6 for SIS0 and SIS1, respectively. The small radius for the SIS0 is to avoid the saturation due to the limit of telemetry. The *EUVE* count rate is extracted from one orbit in a 12' aperture. The Whipple data are limited to be taken at elevations greater than 55°, so that the energy threshold and sensitivity is similar for all runs. Each light curve is normalized to its mean intensity. For TeV data, light curves from three telescopes are first normalized by the flux from the Crab Nebula, and then the combined light curve is normalized.

curve, to 0.195 ± 0.0004 in *ASCA* (0.5–7 keV), to 0.385 ± 0.001 and 0.67 ± 0.03 for 8–16 and 16–40 keV in the *RXTE* Proportional Counter Array data, respectively. This energy dependence is clear in the multiepoch multifrequency spectrum of Mrk 421 shown in Figure 2, where the largest changes in the synchrotron component occur at the highest frequencies.

The complete flare recorded both in X-rays by *BeppoSAX* and in TeV γ -rays by Whipple demonstrates the correlation between X-ray and TeV γ -ray emission on the timescale of hours (Maraschi et al. 1999). The TeV flux also follows the general week-long rise of the *ASCA* flux (Fig. 10 of Takahashi et al. 1999). Assuming the cross-calibration among the three TeV telescopes is accurate, the relative TeV intensities at nearby times indicate that large intraday variations are occurring at these high energies. Fractional TeV variability is 0.30 ± 0.07 for the Whipple data and 0.45 ± 0.08 for the HEGRA data. Note that, for the Whipple data, $F_{\text{var}} = 0.43 \pm 0.05$ during the whole campaign. These values are similar to the values for the hard X-ray data above 8 keV, consistent with the scenario that both TeV and hard X-ray emissions are due to the same electron distribution.

In the subsequent discussion, we divided the *ASCA* light curve into segments as marked in Figure 3, with one flare per segment. In the *ASCA* light curve, most of flares are characterized by nearly equal rise and decay times, i.e., by a nearly symmetric time profile. The time constants from the bottom to the top are also similar from one flare to the next, $\tau \sim 0.5$ days.

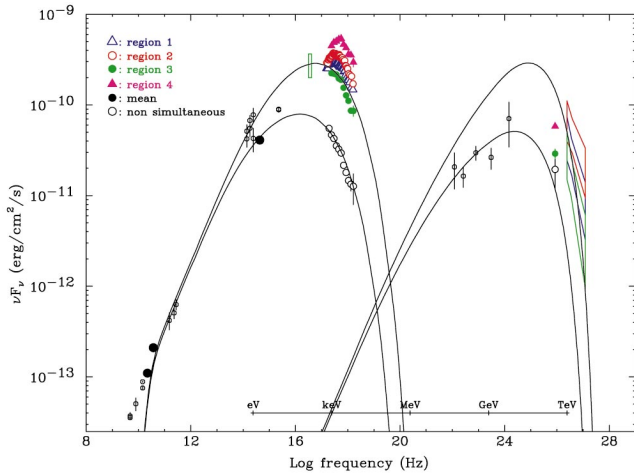


Fig. 2.—Multifrequency spectral energy distribution of Mrk 421 during the 1998 campaign. Filled symbols are simultaneous data obtained during the campaign. Different symbols correspond to different regions defined in Fig. 1. Flux in the 22 GHz, 37 GHz, and R bands are averaged values during the campaign. The box from 0.07–0.2 keV is the range of the flux observed by the *EUVE* during the campaign. Butterfly-shaped boxes in TeV regions are from simultaneous HEGRA observations. The EGRET data are from Macomb et al. (1995), and other data are from the NED database. Lines are predictions by a one-zone synchrotron self-Compton model for the steady state emission (Kataoka 2000). We fixed B to be 0.13 G and δ to be 14. γ_{\max} and electron normalization (per cubic centimeter per second) are $(1.6 \times 10^5, 7.4 \times 10^{-6})$ for the quiescent state and $(2.5 \times 10^5, 5 \times 10^{-5})$ for the high state.

2.3. Time Series Analysis

The long, uninterrupted *ASCA* light curve gives an excellent opportunity to study the temporal characteristics of the X-ray variability. We therefore calculated the first-order *normalized* structure function (SF) at time lag τ , which is defined as $SF(\tau) = (1/N) \sum \{[F(t) - F(t + \tau)]/F_{av}\}^2$, where $F(t)$ is the count rate and F_{av} is the average count rate; N is the total number of data pairs used in the calculation. The SF is closely related to the power density spectrum (PDS) distribution (its slope, β_{SF} , is 1 less than the PDS slope) but is more suitable when the data sampling is uneven. The SF calculated from the 2–7.5 keV *ASCA* light curve is shown in Figure 4. It has a relatively steep slope at high temporal frequencies (short timescales), $\beta_{SF} \sim 1.2$ (corresponding to $\beta_{PDS} \sim 2.2$). This is at the steep end of the slopes seen in other types of mass-accreting black hole systems, such as Seyfert galaxies (Hayashida et al. 1998).

A sharp break in the structure function of Mrk 421 occurs at ~ 0.5 days, to a flatter slope at low temporal frequencies (long timescales), $\beta_{SF} \sim 0.3$ ($\beta_{PDS} \sim 1.3$). This is the first report of a clear turnover in the structure function of a blazar X-ray light curve, and it suggests there is at least one characteristic timescale for the variability of Mrk 421. As shown in Figure 4, the same flat slope at longer lag is seen in the structure function for the *RXTE* all-sky monitor (ASM) light curve (2–10 keV), thus confirming the reality of the turnover. In order for the total variability power not to diverge, the structure function must flatten still further at longer timescales; we infer this from the ASM data to be at ≥ 100 days. The shape of the structure function is roughly independent of energy from 0.07 to 7.5 keV, as can be seen from the comparison of structure functions for the *ASCA* data and the *EUVE* data.

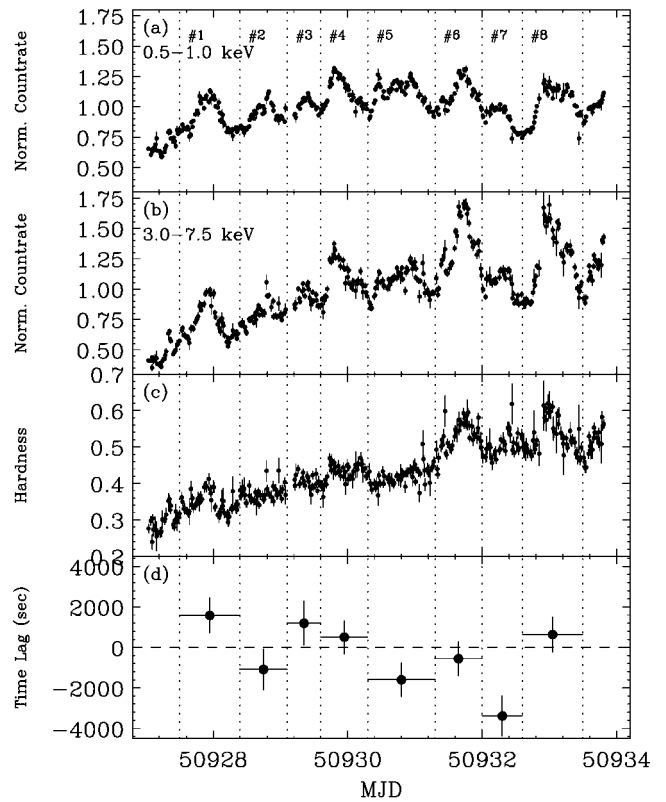


Fig. 3.—Detailed time history of Mrk 421 emission obtained from *ASCA*. Normalized count rate in (a) the 0.5–1.0 keV band and (b) the 3–7.5 keV band. (c) The hardness ratio of count rates, defined as (3–7.5 keV)/(0.5–1.0 keV). (d) Time lag of photons of the 0.5–1 keV band from the 3–7.5 keV band calculated from the DCF. Horizontal bar of each point shows the coverage of data used in the calculation.

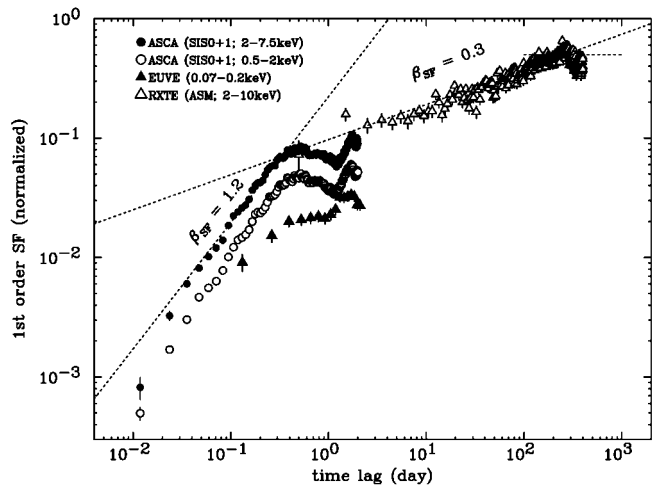


Fig. 4.—Structure function derived from the light curve in the 2–7.5 and 0.5–2 keV bands with *ASCA* (circles) and in the 0.07–0.2 keV band with *EUVE* (filled triangles). Open triangles show the results from ASM data in the 2–10 keV band accumulated from 1996 January 6 to 1999 July 29 but normalized to the mean count rate during the present campaign.

2.4. Spectral Variabilities and Time Lags

The normalized light curves obtained with the SIS in two energy bands (0.5–1 and 3–7.5 keV) are shown in Figures 3a and 3b, respectively. In general, the amplitude of the variability is larger in hard X-rays than in soft X-rays. As can be seen from the hardness ratio (Fig. 3c), the spectrum becomes harder when the source gets brighter. Generally, the spectral changes during individual flares are complex and rapid, but in some cases, the hardness ratio remains almost constant. In flare 8, there is a plateau in the soft X-ray band, which is rarely seen. In order to quantify the lag, we used the discrete correlation function (DCF; Edelson & Krolik 1988). First, we calculated the DCF for the *ASCA* data, comparing each of several energy bands to the 4–7.5 keV band using all data. Our results are consistent with zero lag. We find the same result even using the *EUVE* data, which offers the largest separation in energy from the hard *ASCA* band. However, inspection of X-ray light curves at different energies does suggest some energy dependence of the flare shape. According to detailed analysis of the spectral variability (Kataoka 2000), flare 1 shows clockwise hysteresis in the correlation between flux and photon index, similar to that reported by Takahashi et al. (1996). In contrast, we found anticlockwise hysteresis in flare 7. We therefore calculated the lags separately for each flare (as marked in Fig. 3) to see if individual flares have different behavior.

Figure 3d shows the time lag between 0.5–1 keV photons (the softest *ASCA* band) and 4.0–7.5 keV photons, calculated for each flare. Errors of lags are determined from the quadratic sum of the uncertainty in determining the maximum of the DCF distribution and the results of Monte Carlo calculation, which simulate the effect of time windows (Kataoka 2000). There are both soft (positive) and hard (negative) lags, with some flares consistent with zero. The soft lag for flare 1 is 2000 ± 710 s for 0.5–1.0 keV photons, which is roughly half that found in previous monitoring in 1994 (Takahashi et al. 1996). In contrast, the lag calculated for flare 7 is negative (a hard lag), -3400 ± 980 s. These lags may not be real, as it is not possible to reliably determine lags that are much smaller than an orbit. Systematic effects could also produce these lags.

3. DISCUSSION

The present multiwavelength monitoring campaign showed that Mrk 421 is much more variable and that the variability and its energy dependence is more complex than anticipated. The object flares daily (or perhaps even more often), and the correlation of variations in the X-ray and TeV energy bands is confirmed, supporting the idea that the same electron distribution in the same physical region is responsible for the emission in both energy bands. The 2–7 keV energy index obtained with *ASCA* ranges from $\alpha = 1.4$ to 1.8. The energy ranges covered by *ASCA* and *RXTE* are thus at or above the peak in the νF_ν spectrum. The increasing amplitude of variability at the higher X-ray energies is therefore consistent with the expectations for the synchrotron process, specifically, that the higher energy electrons lose their energy more rapidly.

The X-ray variability of Mrk 421 is very similar to the intraday variability observed in the optical light curves of flat spectrum radio quasars (FSRQs), for which the high-energy component peaks in the GeV γ -ray energy band (Wagner et al. 1996). For synchrotron radiation due to a single population of relativistic electrons with a broken power-law distribution of index γ_{el} and a break at γ_{peak} , the corresponding frequency for γ_{peak} is (as measured in the observer's frame) $\nu_{\text{sync}} =$

$3.7 \times 10^6 \gamma_{\text{peak}}^2 B [\delta/(1+z)]$ Hz. Here B is magnetic field in Gauss, measured in the comoving frame, and δ is the Doppler “beaming” factor defined as $\delta = \Gamma_j^{-1}(1 - \beta \cos \theta)^{-1}$, where Γ_j is the Lorentz factor of the jet, $\beta = v/c$, and θ is the angle of the jet to the line of sight.

Several analyses have shown that γ_{peak} is lower for FSRQs (10^3 – 10^4) and higher for HBLs ($\sim 10^5$ – 10^6), as is the case for Mrk 421 (Sambruna, Maraschi, & Urry 1996; Kubo et al. 1998; Fossati et al. 1998). Since the synchrotron emission due to the electrons with γ_{peak} corresponds to the eV (or sub-eV) range for FSRQs and the keV range for Mrk 421, the rapid, large-amplitude variability observed above γ_{peak} is likely the result of the rapid change of the electron distribution in the regime where acceleration and cooling are approximately balanced (e.g., Inoue & Takahara 1996; Kirk, Rieger, & Mastichiadis 1998). Indeed, the structure function of Mrk 421 derived from the X-ray light curve is very similar to the structure functions found in optical and radio studies of FSRQs, with a break at a characteristic timescale of 1 day (Wagner & Witzel 1995; Wagner et al. 1996).

The *ASCA* light curve constrains the dominant variability timescales to be less than 1 day. The quasi-symmetric flare profiles imply that τ_{acc} and τ_{cool} are shorter than the source light crossing time τ_{crs} , because faster timescales will always be smoothed out by τ_{crs} (Chiaberge & Ghisellini 1999; Kataoka et al. 2000b). A plateau also occurs when the timescale for injecting energetic electrons τ_{inj} is longer than τ_{cool} . In this situation, emission from individual slices does not fade as quickly after an increase; hence, the observation of a plateau in the light curve occurs when the entire volume is radiating. We do observe a plateau in the last flare (segment 8), which is much more obvious at low energies, where the cooling time is longer.

A simple conceptual scenario for multiple flares is that a cloud, or a “blob” of plasma passes through the region where shock fronts are formed and electrons are accelerated. We assume the opening angle of the jet is proportional to $1/\Gamma_j$, where the size of the blob at distance D from the base of the jet can be expressed as $R \sim D/\Gamma_j$. With this, the characteristic timescale of $\tau \sim 0.5$ days (from the structure function analysis) implies that the emission region has size $R = c\tau\Gamma_j \sim 10^{16}$ cm at distance $D \sim 10^{17}$ cm from the black hole, if we assume that $\Gamma_j \sim 10$. Further discussion of the characteristic timescale and a comparison with other TeV blazars and Seyfert galaxies is presented elsewhere (Kataoka et al. 2000a).

If the detection of both positive and negative lags are real, it implies that cooling is sometimes but not always the dominant process and that acceleration is also important. The (familiar) soft lag can be explained by the fact that τ_{cool} is shorter for higher energy electrons [$\tau_{\text{cool}} \propto (1 + u_{\text{soft}}/u_B)^{-1} B^{-2} \gamma^{-1} \delta^{-1}$, where u_B and u_{soft} are the energy densities of the magnetic field and the soft photons to be upscattered, respectively]. When high-energy electrons are injected into the emitting region and then cool radiatively, the soft photons lag the hard, by a time roughly equal to the cooling time at the soft energy (Takahashi et al. 1996). Conversely, the suggested hard lag can be explained, at least qualitatively, if the acceleration time is sufficiently long, $\tau_{\text{acc}} \sim \tau_{\text{cool}}$: electrons appear first at low energies and gradually build up at higher energies (Georganopoulos & Marscher 1998).

The relatively small lags also mean $\tau_{\text{acc}} \sim \tau_{\text{cool}}$ at X-ray energies, at least during the present observations. This is consistent with the fact that the X-ray band is emitted by the highest energy regime of the electron distribution, where τ_{acc} is approximately balanced with τ_{cool} . According to the shock acceleration scenario,

τ_{acc} depends on energy in an opposite sense to τ_{cool} . It follows $\tau_{\text{acc}}(\gamma) \propto \gamma$ for diffusive acceleration with a “gyro-Bohm” process (e.g., Inoue & Takahara 1996) or $\tau_{\text{acc}}(\gamma) \propto \gamma^{1/3}$ for fully developed Kolmogorov turbulence. Similar discussions have been made by several authors (e.g., Sambruna 2000).

At a minimum, the present observations underline the need for detailed time-dependent synchrotron models, in which the timescales for electron acceleration and injection, and for radiative cooling and escape, are free to vary (e.g., Kirk et al. 1998). Depending on the relative values of these timescales, a

variety of behaviors can be expected in the light curves. The fact that plateaus are rarely seen implies the dominant timescale is similar to the light crossing time, which in turn supports the idea that the size of the emitting region is determined by diffusion and cooling.

C. M. U. acknowledges support from NASA grant NAG5-3313. G. M. acknowledges NASA grants to USRA and the University of Maryland.

REFERENCES

- Aharonian, F., et al. 1999, *A&A*, 349, 29
 Buckley, J. H., et al. 1996, *ApJ*, 472, L9
 Chiaberge, M., & Ghisellini, G. 1999, *MNRAS*, 306, 551
 Edelson, R. A., & Krolik, J. H. 1988, *ApJ*, 333, 646
 Fossati, G., et al. 1998, *MNRAS*, 299, 433
 ———. 2000a, *ApJ*, 541, 153
 ———. 2000b, *ApJ*, 541, 166
 Georganopoulos, M., & Marscher, A. P. 1998, *ApJ*, 506, L11
 George, I. M., Warwick, R. S., & Bromage, G. E. 1988, *MNRAS*, 232, 793
 Ghisellini, G., et al. 1998, *MNRAS*, 301, 451
 Hayashida, K., et al. 1998, *ApJ*, 500, 642
 Inoue, S., & Takahara, F. 1996, *ApJ*, 463, 555
 Kataoka, J. 2000, Ph.D. thesis, Univ. Tokyo
 Kataoka, J., et al. 2000a, *ApJ*, submitted
 ———. 2000b, *ApJ*, 528, 243
 Kirk, J. G., Rieger, F. M., & Mastichiadis, A. 1998, *A&A*, 333, 452
 Kubo, H., et al. 1998, *ApJ*, 504, 693
 Macomb, D., et al. 1995, *ApJ*, 449, L99 (erratum 459, L111 [1996])
 Maraschi, L., et al. 1999, *ApJ*, 526, L81
 Sambruna, R. M. 2000, *Mem. Soc. Astron. Italiana*, in press (astro-ph/9912060)
 Sambruna, R. M., Maraschi, L., & Urry, C. M. 1996, *ApJ*, 463, 444
 Takahashi, T., Madejski, G., & Kubo, H. 1999, *Astropart. Phys.*, 11, 177
 Takahashi, T., et al. 1996, *ApJ*, 470, L89
 Teräsranta H., et al. 1998, *A&AS*, 132, 305
 Ulrich, M.-H., Maraschi, L., & Urry, C. M. 1997, *ARA&A*, 35, 445
 Urry, C. M., & Padovani, P. 1995, *PASP*, 107, 803
 Wagner, S. J. 1996, *A&AS*, 120, 495
 Wagner, S. J., et al. 1996, *AJ*, 111, 2187
 Wagner, S. J., & Witzel, A. 1995, *ARA&A*, 33, 163